A novel Pyrin-Associated Autoinflammation with Neutrophilic Dermatosis mutation further defines 14-3-3 binding of Pyrin and distinction to Familial Mediterranean Fever

Fiona Moghaddas MBBS[1,2], Rafael Llamas MD[3], Dominic De Nardo PhD[1,2], Helios Martinez-Banaclocha BSc[4], Juan J. Martinez-Garcia BSc[4], Pablo Mesa-del-Castillo MD[4,5], Paul J. Baker BSc[1,2], Vanessa Gargallo MD[3], Anna Mensa-Vilaro MD[6], Scott Canna MD[7], Ian P. Wicks MBBS PhD[1, 2, 8], Pablo Pelegrin PhD[4], Juan I. Arostegui MD PhD[6,*], Seth L. Masters PhD[1,2,#,*]

[1] Inflammation Division, The Walter and Eliza Hall Institute of Medical Research, Parkville, Australia

[2] Department of Medical Biology, The University of Melbourne, Parkville, Australia

[3] Department of Dermatology, Hospital Universitario 12 de Octubre, Madrid, Spain

[4] Inflammation and Experimental Surgery Unit, Biomedical Research Institute of Murcia (IMIB-Arrixaca), Hospital Clinico Universitario Virgen de la Arrixaca, El Palmar, Murcia, Spain

[5] Department of Rheumatology, University Clinical Hospital Virgen de la Arrixaca, Murcia, Spain

[6] Department of Immunology-CDB, Hospital Clinic-IDIBAPS, Barcelona, Spain

[7] Pediatric Rheumatology/RK Mellon Institute, Children's Hospital of Pittsburgh of UPMC, Pittsburgh, PA

[8] Rheumatology Department, The Royal Melbourne Hospital, Parkville, Australia

∗ Co-senior author

Corresponding author: masters@wehi.edu.au

Abstract

Objective: Pyrin-Associated Autoinflammation with Neutrophilic Dermatosis (PAAND) is a recently described monogenic autoinflammatory disease. The causal p.S242R *MEFV* mutation disrupts a binding motif of the regulatory 14-3-3 proteins within pyrin. Here we investigate a family with clinical features consistent with PAAND in whom the novel p.E244K *MEFV* mutation, located in the +2 site of the 14-3-3 binding motif in pyrin, has been found.

Methods: Multiplex cytokine analyses were performed on p.E244K patient and control serum. Peripheral blood mononuclear cells were stimulated *ex vivo* with LPS. *In vitro*, inflammasome complex formation was evaluated by flow cytometry of Apoptosis-associated Speck-like protein containing a Caspase recruitment domain (ASC) specks. IL-1β and IL-18 production was quantified by enzyme-linked immunosorbent assay (ELISA). The ability of the p.E244K pyrin mutation to interact with 14-3-3 was assessed by immunoprecipitation.

Results: PAAND p.E244K patient serum displays a different cytokine profile compared to patients with Familial Mediterranean Fever (FMF). In overexpression models, p.E244K pyrin was associated with decreased 14-3-3 binding and increased ASC speck formation. THP-1 monocytes expressing PAAND pyrin mutations demonstrated spontaneous caspase-1-dependent IL-1β and IL-18 secretion, as well as cell death, which were significantly greater than those of wild type and the FMF-associated mutation p.M694V.

Conclusion: In PAAND, disruption of the +2 position of a 14-3-3 binding motif in pyrin results in its constitutive activation, with spontaneous production of IL-1β and IL-18, associated with inflammatory cell death. The altered serum cytokine profile may explain the different clinical features exhibited by PAAND patients compared to those with FMF.

Keywords: Pyrin, PAAND, Autoinflammatory Disease, 14-3-3, FMF

Introduction

Pyrin-Associated Autoinflammation with Neutrophilic Dermatosis (PAAND) is a recently described monogenic autoinflammatory condition caused by a heterozygous mutation in the *MEFV* gene resulting in the p.S242R substitution in pyrin (1). The dominant clinical phenotype of prolonged fever and neutrophilic dermatosis (e.g. acne, pyoderma gangrenosum), and potentially the mechanism of disease, differs from the classical pyrin-associated disease, Familial Mediterranean Fever (FMF).

The p.S242 site of pyrin forms a 14-3-3 binding motif (1, 2). Although there are a number of variations of 14-3-3 recognition motifs reported, all contain a phosphorylated serine or threonine residue (3, 4). In its inactive state, pyrin is phosphorylated by serine-threonine kinases PKN1 and PKN2 at residues p.S208 and p.S242, and is bound to 14-3-3 proteins (5). When triggered in response to RhoGTPase modifications, such as those induced by the pathogen *Clostridium difficile*, there is dephosphorylation of pyrin at p.S208 and p.S242 residues and loss of 14-3-3 binding (1, 5, 6). *In vitro* models show that the p.S242R pyrin mutation is constitutively dephosphorylated, with reduced 14-3-3 binding (1). The resulting increased pyrin inflammasome activation and enhanced IL-1β production appear to drive the pathology in PAAND (1).

Here, we report a novel mutation in the *MEFV* gene in a family with clinical features of PAAND that results in an altered 14-3-3 binding motif and constitutive activation of pyrin. We also confirm phenotypic differences and identify cytokine differences between PAAND and FMF.

Methods

Patients

We investigated three symptomatic patients in one family. We used patients with homozygous p.M694V FMF as disease controls, and blood donors as healthy controls. This study was approved by the Hospital Clinic-IDIBAPS Ethics Committee.

Patient cell stimulation and analysis

Fresh serum samples were collected from patients and controls, and cytokine quantification was performed by Luminex Multiplex Assay. PAAND patients had active clinical features at the time of collection. For human IL-18 and IL-18BP, serum was assayed in multiplex on a Luminex Magpix system (Bio-Rad). Bio-Rad group II cytokine standard was used for IL-18, whereas recombinant human IL-18BPa-Fc chimeric protein (R&D Systems) was used as standard for IL-18BP.

Peripheral blood mononuclear cells (PBMCs) were isolated using Histopaque-1077 (Sigma-Aldrich) and treated with *E. coli* LPS serotype 055:B5 (Sigma-Aldrich; 1 μg/ml, 2h at 37°C) or left untreated. IL-1β was measured on cell supernatants by enzyme-linked immunosorbent assay (ELISA, eBiosciencies) whilst other cytokine quantification was performed by Luminex Multiplex Assay as described above. Cells were fixed with 2% paraformaldehyde and stained for the detection of Apoptosis-associated Speck-like protein containing a Caspase recruitment domain (ASC) specks by Time of Flight Inflammasome Evaluation (TOFIE) using the rabbit polyclonal antibody anti-ASC (N-15)-R (Santa Cruz Biotechnology) as previously described (7). Alternatively, for the detection of active caspase-1, PBMCs were incubated for 20 min with FLICA660 reagent (ImmunoChemistry Technologies) and fixed following

manufacturer's recommendations. Monocytes were detected with the APC-vio770 mouse anti-human CD33 antibody (Miltenyi Biotech) and with the APC-Cy7-conjugated anti-human CD14 antibody (TONBO biosciences). Stained cells were acquired on a BD FACS-Canto cytometer.

Heat maps representing cytokine expression profiles were created using Morpheus software (Broad Institute).

Cell culture

HEK293T cells were cultured in DMEM supplemented with 10% FCS and transfected with mCherry- or GST-pyrin (8), GFP-ASC (9), or V5-PSTPIP1 (HsCD00438559, DNASU Plasmid repository) constructs using Lipofectamine (Life Technologies) according to manufacturer's instructions. CRISPR/Cas9 techniques were used for generation of *MEFV* KO and *CASP1* KO THP-1 cells, as has been described(1, 10). These cells were cultured in RPMI supplemented with 10% FCS.

Lentiviral infection of THP-1 cells

MEFV KO THP-1 cells were reconstituted with pyrin by lentiviral transduction. A lentiviral construct was generated through ligation of *MEFV* cDNA into *Bam*HI and *Age*I restriction sites on the pFUGW backbone after performing site directed mutagenesis of the *Bam*HI restriction site within *MEFV*. Lentivirus was produced as previously described (10). One million THP-1 cells were seeded per well in 6-well plates with 3.5mL of virus and 24μg of polybrene. A total of 6 million THP-1 cells were seeded per condition. Plates were centrifuged at 840g for 3h and then incubated at 37°C overnight. Cells were collected the following day, washed in PBS, reseeded in fresh media and incubated at 37°C overnight. After a further 24h, live and dead cells were separated using Ficoll density gradient centrifugation (GE Healthcare). Live cells

were seeded for experiments. Supernatant was harvested after 24h for cytokine analysis by ELISA for IL-1β and IL-18 (DY201 and DY008, R&D Systems). Cytokines from cell culture supernatant were also quantified using Bio-Plex Pro Assay (Bio-Rad). Cell death was analysed by flow cytometry using propidium iodide (Sigma-Aldrich) staining at 1μg/ml. Where indicated, priming of cells was performed with Pam3CSK4, a synthetic TLR1/2 agonist (Invivogen). Cells were also lysed using Radioimmunoprecipation assay (RIPA) buffer to assess expression of pyrin by western blotting.

Site directed mutagenesis

Site directed mutagenesis was performed using the QuickChange Lightning Kit (210519-5, Agilent Technologies) according to manufacturer's instructions. Mutations were introduced to pyrin-expressing constructs using the following oligonucleotide primers:

p.E244K	5'-TAGAAATGGTGACCTTAAGGCTTCTAGGTCGCATC-3'
	5'-GATGCGACCTAGAAGCCTTAAGGTCACCATTTCTA-3'
p.M694V	5'-GGTACTCATTTTCCTTCACCATTATCACCACCCAGTAG-3'
	5'-CTACTGGGTGGTGATAATGGTGAAGGAAAATGAGTACC-3'
p.S242R	5'-GAAATGGTGACCTCAAGCCTTCTAGGTCGCATCTT-3'
	5'-AAGATGCGACCTAGAAGGCTTGAGGTCACCATTTC-3'
p.E244P	5'-GATGCGACCTAGAAGCCTTCCGGTCACCATTTCTACAG-3'
	5'-CTGTAGAAATGGTGACCGGAAGGCTTCTAGGTCGCATC-3'
p.E244D	5'-CGACCTAGAAGCCTTGATGTCACCATTTCTACAGG-3'
	5'-CCTGTAGAAATGGTGACATCAAGGCTTCTAGGTCG-3'
p.E244R	5'AGATGCGACCTAGAAGCCTTAGGGTCACCATTTCTACAGG-3'
	5'-CCTGTAGAAATGGTGACCCTAAGGCTTCTAGGTCGCATCT-3'
R39R*(*Δ*Bam*HI)	5'-GGAGCACTCCAGAATCCCCCGGAGC-3'

		5’-GCTCCGGGGGATTCTGGAGTGCTCC-3’
I666I*(ΔBam*HI)		5’-CAGGCTCCCAGTATCCATGCTGTCTTGTCTCC-3’
		5’-GGAGACAAGACAGCATGGATACTGGGAGCCTG-3’

Fluorescence microscopy and flow cytometry

HEK293T cells were transfected with 25ng WT or mutant mCherry-MEFV and 5ng GFP-ASC, and ASC specks were quantified 16h later using flow cytometry, as previously described (7). Colocalisation experiments were performed using mCherry-MEFV and GFP-ASC transfected into $1x10^5$ HEK 293T cells seeded in ibidi chamber slides (ibidi GmbH). Images were taken with a Zeiss LSM 780 Confocal microscope and were processed using FIJI software (NIH).

Immunoprecipitation and western blotting

HEK293T cells ($3x10^6$ cells) were transfected with 5μg of GST-tagged WT or mutant pyrin, with or without WT PSTPIP1. Where indicated, cells were treated with *Clostridium difficile* Toxin B protein (TcdB, 5μg/ml, Abcam ab124001) 16h before harvesting. Cell lysates were generated 48h after transfection using 1% NP-40 lysis buffer supplemented with protease inhibitors and sodium orthovanadate. Immunoprecipitation of pyrin was performed using glutathione sepharose 4B (GE healthcare). After washing, bound proteins were eluted from beads using 2x SDS buffer and boiling at 90°C. Immunoblots were prepared using 4-12% SDS-PAGE (Novex) gels in MES running buffer, followed by transfer on to nitrocellulose membranes. Membranes were blocked with TBST + 3% BSA at room temperature and subsequently probed overnight at 4°C with antibodies against pan-14-3-3 (1:500 Santa Cruz #sc-629-G), 14-3-3τ (1:500 SantaCruz #sc-59414), 14-3-3ε (1:1000 Biorbyt #orb6357), pSer 14-3-3 binding motif (1:500 Cell signaling #9601), pyrin (1:500 AdipoGen #AL196), p10 Caspase-1 (1:200 Santacruz #sc-515), IL-1β (1:1000 R&D #AB-401-NA), GST (1:1000 in-

177 house), PSTPIP1 (1:500 Abnova #H00009051); and actin (1:5000 Santa Cruz #sc-1616). All
178 antibodies were prepared in TBST + 1% BSA.
179
180 ***Statistical analysis***
181 Mann Whitney non-parametric test was used for the analysis of data in Figure 2. Two-tailed *t*
182 tests were performed in other analysis using Prism software (GraphPad). Data is represented
183 as mean +/- SEM unless otherwise specified. *$P < 0.05$, **$P < 0.01$, ***$P < 0.001$, ****P
184 < 0.0001.

Results

PAAND family with a novel mutation in *MEFV*.

The index patient is a 43-year-old female of Spanish descent with a thirty-year history of chronic and severe pustular acne, severe hidradenitis suppurativa, recurrent pyoderma gangrenosum, recurrent long-lasting febrile episodes, neutrophilic panniculitis, as well as polyarthralgia and oligoarthritis of small and large joints **(Figure 1A)**. Raised C-reactive protein (CRP) and Erythrocyte Sedimentation Rate (ESR), and increased peripheral blood neutrophil count persisted despite treatment with corticosteroids and the IL-1 receptor antagonist (IL-1Ra), Anakinra **(Figure 1B)**. Long-lasting (8 years) clinical benefit was seen with the chimeric anti-TNF-α monoclonal antibody Infliximab. However, loss of efficacy for Infliximab was observed and necessitated switching to the human anti-TNF-α monoclonal antibody Adalimumab when symptoms recurred. Although a clinical diagnosis of Pyogenic Arthritis, Pyoderma Gangrenosum and Acne (PAPA) syndrome was suspected, genetic testing of *PSTPIP1* failed to reveal a pathogenic mutation. Pathogenic mutations in *NCSTN,* reported in familial cases of hidradenitis suppurtiva, were absent (11). The recent description of PAAND, a condition with significant clinical overlap with PAPA syndrome, prompted exon 2 *MEFV* sequencing in this patient, which revealed the heterozygous c.730G>A transition in the *MEFV* gene encoding for the p.E244K mutation (**Figure 1C**). This mutation was absent from the 1000 Genomes Project, Exome Aggregatium Consortium (ExAC), Exome Variant Server and 250 Spanish healthy controls. Furthermore, it had not been reported on the INFEVERS database (12-14). The locus is highly conserved across species **(Figure 1D)** and the amino acid substitution predicted to be damaging using Mutation Taster (15), Sorting Intolerant from Tolerant (SIFT) (16), and Polymorphism Phenotyping v2 (PolyPhen-2) (17). Evaluation of the patient's mother and brother, both of whom have had dermatitis and long-lasting (>30 years) severe nodulocystic acne affecting the face and trunk respectively, revealed the mutation of

interest, suggesting an autosomal dominant disease with variable penetrance (see online supplementary **Figure S2**).

PAAND family has a cytokine profile distinct from FMF patients.

Serum cytokine analysis of the proband, mother and brother revealed a unique profile when compared to FMF patients (n=5) and healthy controls (n=7), highlighted on a heat map of relative values (**Figure 2A**). The increased serum IL-18 was explored further with the measurement of IL-18 binding protein (IL-18BP). IL-18BP has a high affinity for IL-18, and renders it biologically inactive (18). Free IL-18, rather than total, correlates better with disease activity in IL-18-driven conditions, such as haemophagocytic lymphohistiocytosis (19). Interestingly, in our PAAND patients, IL-18BP was significantly elevated when compared with healthy controls, and the ratio of total IL-18 to IL-18BP was similar (**Figure 2B**). Therefore, analysis of free IL-18 revealed no significant increase (data not shown).

When activated, most inflammasomes, including pyrin, associate with the adaptor protein ASC to form a platform for procaspase-1 activation and cleavage of pro-IL-1β and pro-IL-18 to the mature forms (20, 21). Monocytes isolated from PAAND patients showed increased ASC speck formation with LPS exposure, and there is a trend toward an increase at baseline (**Figure 2C**). Caspase-1 activity as measured by YVAD-FLICA staining was increased in PAAND monocytes when treated with LPS (**Figure 2D**). Given these results it was surprising that IL-1β production from PAAND patient PBMCs in response to LPS was unaltered (**Figure 2E**). Nevertheless, the total IL-18 secreted by PBMCs was increased compared with healthy controls, both at baseline and following LPS stimulation, as were levels of IL-1Ra (**Figures 2F and 2G**).

p.E244K pyrin is associated with increased ASC speck formation.

To determine whether the above results were indeed caused by the novel p.E244K pyrin mutation, we assessed ASC speck formation *in vitro* as a surrogate marker for inflammasome formation. Colocalisation experiments were performed by expression of both mCherry-tagged pyrin and GFP-ASC in HEK293T cells (**Figure 3A**). There was minimal spontaneous ASC speck formation. As expected, WT pyrin augmented this response, but p.E244K pyrin did so further (**Figure 3B**). This was quantified using flow cytometry (see online supplementary **Figure S3**), with p.E244K pyrin resulting in a similar percentage of cells with ASC speck formation compared with the other known PAAND mutation p.S242R, both of which were greater than WT and p.M694V pyrin (**Figures 3C and 3D**).

p.E244K pyrin is associated with increased IL-1β, IL-18, and pyroptosis.

Further functional studies were performed using THP-1 monocytes. *MEFV* KO or *CASP1* KO THP-1 cells were reconstituted with *MEFV* using lentiviral transduction of WT or mutant cDNA . Even without stimulation, *MEFV* KO THP-1 cells expressing p.E244K pyrin displayed increased cell death (**Figure 4A**), as well as IL-1β and IL-18 release (**Figures 4B and 4C**). Surprisingly, this phenotype was present without "priming" the inflammasome, which is usually required to induce pro-IL-1β expression (22). Interestingly, IL-1β production in both p.E244K and p.S242R pyrin-expressing *MEFV* KO THP-1 cells was significantly higher than cells expressing FMF associated p.M694V pyrin (**Figure 4C**). Genetic deletion of caspase-1 prevented p.E244K and p.S242R pyrin-induced cytokine production as well as cell death, suggesting the caspase-1 dependent inflammatory cell death (pyroptosis) (**Figures 4A, 4B and 4C**). However, genetic deletion of caspase-1 did not affect P3CSK4-induced-priming of pro-IL-1β (**Figure 4D**). These *in vitro* data support the hypothesis that inflammasome activation in p.E244K pyrin patients is responsible for excessive cytokine release and pyroptosis .

p.E244K pyrin does not alter PSTPIP1 binding.

In PAPA syndrome, mutant PSTPIP1 is hyperphosphorylated and binds more strongly to pyrin (23). Given the clinical similarities between PAAND and PAPA syndrome, binding of PSTPIP1 to pyrin with and without PAAND mutations was assessed. Both GST-pyrin and PSTPIP1 were transfected into HEK293T cells and GST-immunoprecipitation performed. When comparing the binding of WT PSTPIP1 to WT, PAAND and FMF associated pyrin, no significant difference was observed. This suggests that the mechanism of this disease is not related to increased PSTPIP1 binding (see online supplementary **Figure S4**).

p.E244K pyrin has reduced phosphorylation of 14-3-3 binding motif and reduced 14-3-3 binding.

The initial report of PAAND showed that the mechanism of increased inflammasome activation was loss of 14-3-3 binding to pyrin and subsequent loss of autoinhibition (1). Given that p.E244 is the +2 position of a 14-3-3 binding motif (**Figure 1D**), preliminary experiments were conducted to examine 14-3-3 binding to p.E244K pyrin. Serine residues at positions p.S208 and p.S242 have previously been shown to interact with 14-3-3 (1, 2), and were used as comparators. Immunoprecipitation was performed using GST-tagged WT and mutant pyrin transfected into HEK293T cells. This revealed reduced binding of an antibody that recognizes phosphorylated serine in the 14-3-3 binding motif in mutants p.E244K and p.S242R pyrin, but not in the FMF associated p.M649V pyrin (**Figure 5A**). Binding of 14-3-3 to pyrin was also affected, following the same pattern. Further evaluation of binding of the 14-3-3τ and 14-3-3ε isoforms to these mutants, as well as p.S208A and p.S208A/S242R pyrin, showed no differences, suggesting both isoforms behave similarly **(Figure 5B)**. These data suggest that PAAND pyrin mutations result in reduced phosphorylation of the 14-3-3 binding motif and reduced 14-3-3 binding to pyrin.

The p.E244 position is important in 14-3-3 binding to pyrin.

Phosphorylated serine in specific motifs is important for 14-3-3 binding. Previous reports had suggested that proline was required at the +2 position of the motif for interaction between 14-3-3s and their target protein, documented as RXX(pS)XP **(Figure 1D)**. However, subsequent reports show that proline in +2 position is present in only 50% of 14-3-3 binding motifs (24). To explore the importance of the +2 position in 14-3-3 binding and pyrin regulation, p.E244 pyrin was mutated to various amino acids. Glutamate (E) was substituted by aspartate (D) or arginine (R) to explore charge and polarity respectively; or proline (P) to explore the effect of the canonical 14-3-3 binding motif. Flow cytometric analysis of these mutants showed an increase in ASC speck formation in p.E244R pyrin mutant, while p.E244D and p.E244P pyrin mutations did not further activate pyrin in this assay (**Figure 6A**). Immunoprecipitation showed that p.E244R pyrin had reduced binding to 14-3-3 when compared to WT, similar to p.E244K (**Figure 6B**). Interestingly, p.E244P pyrin had increased 14-3-3 binding, suggesting that this mutation could potentially suppress pyrin activation. To test this hypothesis, cells were treated with the RhoGTPase inhibitor, TcdB, to activate pyrin. Although p.E244P increased binding of 14-3-3 to pyrin, this was insufficient to prevent activation by TcdB (**Figure 6C**). Furthermore, the double mutant p.E244P/M694V had no effect on this, highlighting again a distinct pathophysiologic mechanism of FMF and PAAND (**Figure 6C**).

Discussion

The initial clinical suspicion of PAPA syndrome in the index patient highlights the striking clinical overlap between PAAND and PAPA syndrome, as noted in the original description of PAAND (1). Compared with the initial report, our family is distinct in suffering from polyarthritis as well as severe hidradenitis suppurativa, suggesting that even within the PAAND diagnosis, there is variability in clinical presentation, consistent with a spectrum of pyrin-associated features. Our results agree with the original description of PAAND, namely that excessive IL-1β is pyrin-dependent. Although PAPA syndrome is also pyrin-dependent (23), the exact mechanisms underlying the similar clinical presentations of PAAND and PAPA syndrome have not been elucidated. We suggest that patients with clinically suspected PAPA syndrome who test negative for *PSTPIP1* mutations should undergo genetic evaluation of *MEFV,* with particular attention to the bases in exon 2 encoding 14-3-3 binding motifs.

The role of 14-3-3 in controlling the activation of pyrin is highlighted by this novel mutation causing PAAND. Reduced binding of 14-3-3 to pyrin was seen with both p.E244K and p.S242R pyrin, but not in the FMF-associated p.M694V mutation (**Figure 5**). The loss of 14-3-3 binding following stimulation with TcdB suggests that 14-3-3 is required to maintain pyrin in an auto-inhibited state and reduced 14-3-3 binding to PAAND-associated pyrin leads to its auto-activation. We propose that, with the same expression of pyrin across the mutants examined in our model, the PAAND pyrin is likely to be more active, with increased pyroptosis and availability of pro-IL-1 for cleavage. It is possible that PAAND is at one spectrum of pyrin associated disorders in terms of severity, with PAAND pyrin being spontaneously active and FMF pyrin having a lower threshold for activation than WT pyrin.

The 14-3-3 binding motif of pyrin differs from the canonical RXX(pS)XP motif with a highly conserved glutamate at the +2 position. Substituting glutamate for proline or aspartate, nonpolar and negatively charged amino acids respectively, retained 14-3-3 binding to pyrin, whereas substitutions to lysine or arginine, both positively charged amino acids, do not appear to be tolerated. The structure of this region of pyrin has not been elucidated, making it difficult to predict the effect of amino acid substitutions. However, we demonstrate that the +2 position of the 14-3-3 binding motif is important, and that substitution at this site can alter the ability for 14-3-3 to bind to pyrin.

Although M694V pyrin results in increased inflammasome formation (25), the mechanism of auto-activation still remains to be elucidated. We saw no discernable difference between WT and p.M694V pyrin with regards to 14-3-3 binding, and Van Gorp *et al.,* documented unaltered phosphorylation at position p.S242 in p.M694V pyrin transfected HEK293T cells, which is required for 14-3-3 binding (26). Interestingly, Park *et al.*, did see reduced 14-3-3ε binding in FMF-associated mutations(5). It is possible that subtle differences in the experimental approach may influence this result, and given that PAAND is a more severe disease, we would expect FMF mutations to have a smaller mechanistic effect on 14-3-3 binding.

In addition to 14-3-3 binding, the clinical presentation, mode of inheritance, and biochemical status of PAAND differs from FMF. Although this study focuses on only two generations of one family, the heterozygous mutation and variable phenotype suggests a dominant disorder with variable penetrance, compared with the typically autosomal recessive inheritance of FMF. All members of the PAAND family have marked dermatological manifestations, further differentiating this condition from FMF.

Another distinction between these pyrin-associated conditions is evident from the serum cytokine profile, and cytokine production by PBMCs, both at baseline and after LPS-priming. Although the FMF patients were asymptomatic, there was evidence of systemic inflammation with raised CRP in four of the five controls (see online supplementary **Table S1**). Furthermore, their serum cytokine profile was distinct from healthy controls as well as PAAND patients, suggesting that there are indeed differences that are not accounted for by symptom control.

Despite elevated IL-1β in these analyses, one patient with the p.E244K mutation did not improve with a trial of anakinra. Interestingly, the elevated IL-1Ra levels in this individual may explain why a recombinant IL-1Ra did not provide further benefit. Our FMF patients did not have elevated IL-1Ra levels, and a number of recent publications suggest that colchicine-resistant FMF can be adequately treated with IL-1 antagonism (27-29). Despite elevated IL-18 levels in PAAND PBMC secreted at baseline and in response to LPS **(Figures 2F)**, an increase in IL-18BP levels **(Figure 2B)** suggests that targeting this pathway may not be as effective as shown for patients with activation of the NLRC4 inflammasome (30). The clinical response to TNF inhibition in our patient suggests that this is an important cytokine in PAAND, even though TNF was not elevated in the serum of these patients. This may be because at the time of the study the patient was receiving treatment with immunomodulatory drugs including Adalimumab. Alternatively, increased cell death in PAAND (**Figure 4A**) could release damage associated molecular patterns (DAMPs) that trigger local cytokine production in tissues such as the skin. Furthermore, it would be interesting to assess tissue specific cytokines and cell responses, as these may reveal pathogenic factors not present in peripheral blood. Regardless, given the difficulty controlling disease activity and the need for multiple therapeutic agents, PAAND is likely to be driven by more than a single cytokine.

The p.E244K pyrin mutation in PAAND patients highlights the importance of the 14-3-3 binding motif in pyrin activation, in addition to the p.S242R mutation described originally. Our study suggests that although PAAND and FMF mutations are located in the same gene, they are distinct diseases clinically, with unique cytokine profiles, cellular responses and 14-3-3 binding.

Acknowledgements: We thank the patient and family for participation in this study.

Funding:

I.P.W.: Australian National Health and Medical Research Council Program (NHMRC) project grant (1113577)

P.P.: Grants from *Instituto Salud Carlos III-FEDER* (PS13/00174) and European Research Council (ERC-2013-CoG 614578). P.P. would like to acknowledge networking support by the COST Action BM-1406.

H.M-B: Rio Hortega fellowship from *Instituto Salud Carlos III* (CM14/00008),

J.I.A.: CERCA Programme/Generalitat de Catalunya and SAF2015-68472-C2-1-R grant from the Spanish Ministry of Economy and Competitiveness and Fondo Europeo de Desarrollo Regional (FEDER).

S.L.M.: NHMRC projects grants (1099262, 1081299) Viertel Fellowship and funding from Glaxosmithkline.

References

1. Masters SL, Lagou V, Jeru I, Baker PJ, Van Eyck L, Parry DA, et al. Familial autoinflammation with neutrophilic dermatosis reveals a regulatory mechanism of pyrin activation. Science translational medicine. 2016;8(332):332ra45.

2. Jeru I, Papin S, L'Hoste S, Duquesnoy P, Cazeneuve C, Camonis J, et al. Interaction of pyrin with 14.3.3 in an isoform-specific and phosphorylation-dependent manner regulates its translocation to the nucleus. Arthritis Rheum. 2005;52(6):1848-57.

3. Obsilova V, Nedbalkova E, Silhan J, Boura E, Herman P, Vecer J, et al. The 14-3-3 protein affects the conformation of the regulatory domain of human tyrosine hydroxylase. Biochemistry. 2008;47(6):1768-77.

4. Obsilova V, Silhan J, Boura E, Teisinger J, Obsil T. 14-3-3 proteins: a family of versatile molecular regulators. Physiological research / Academia Scientiarum Bohemoslovaca. 2008;57 Suppl 3:S11-21.

5. Park YH, Wood G, Kastner DL, Chae JJ. Pyrin inflammasome activation and RhoA signaling in the autoinflammatory diseases FMF and HIDS. Nat Immunol. 2016;17(8):914-21.

6. Xu H, Yang J, Gao W, Li L, Li P, Zhang L, et al. Innate immune sensing of bacterial modifications of Rho GTPases by the Pyrin inflammasome. Nature. 2014;513(7517):237-41.

7. Sester DP, Thygesen SJ, Sagulenko V, Vajjhala PR, Cridland JA, Vitak N, et al. A novel flow cytometric method to assess inflammasome formation. J Immunol. 2015;194(1):455-62.

8. Chae JJ, Komarow HD, Cheng J, Wood G, Raben N, Liu PP, et al. Targeted disruption of pyrin, the FMF protein, causes heightened sensitivity to endotoxin and a defect in macrophage apoptosis. Molecular cell. 2003;11(3):591-604.

9. Waite AL, Schaner P, Richards N, Balci-Peynircioglu B, Masters SL, Brydges SD, et al. Pyrin Modulates the Intracellular Distribution of PSTPIP1. PloS one. 2009;4(7):e6147.

10. Baker PJ, Boucher D, Bierschenk D, Tebartz C, Whitney PG, D'Silva DB, et al. NLRP3 inflammasome activation downstream of cytoplasmic LPS recognition by both caspase-4 and caspase-5. Eur J Immunol. 2015;45(10):2918-26.

11. Wang B, Yang W, Wen W, Sun J, Su B, Liu B, et al. Gamma-secretase gene mutations in familial acne inversa. Science. 2010;330(6007):1065.

12. Touitou I, Lesage S, McDermott M, Cuisset L, Hoffman H, Dode C, et al. Infevers: an evolving mutation database for auto-inflammatory syndromes. Hum Mutat. 2004;24(3):194-8.

13. Sarrauste de Menthiere C, Terriere S, Pugnere D, Ruiz M, Demaille J, Touitou I. INFEVERS: the Registry for FMF and hereditary inflammatory disorders mutations. Nucleic Acids Res. 2003;31(1):282-5.

14. Milhavet F, Cuisset L, Hoffman HM, Slim R, El-Shanti H, Aksentijevich I, et al. The infevers autoinflammatory mutation online registry: update with new genes and functions. Hum Mutat. 2008;29(6):803-8.

15. Schwarz JM, Cooper DN, Schuelke M, Seelow D. MutationTaster2: mutation prediction for the deep-sequencing age. Nature methods. 2014;11(4):361-2.

16. Kumar P, Henikoff S, Ng PC. Predicting the effects of coding non-synonymous variants on protein function using the SIFT algorithm. Nat Protoc. 2009;4(7):1073-81.

17. Adzhubei I, Jordan DM, Sunyaev SR. Predicting functional effect of human missense mutations using PolyPhen-2. Current protocols in human genetics. 2013;Chapter 7:Unit7.20.

18. Dinarello CA, Novick D, Kim S, Kaplanski G. Interleukin-18 and IL-18 Binding Protein. Front Immunol. 2013;4.

19. Mazodier K, Marin V, Novick D, Farnarier C, Robitail S, Schleinitz N, et al. Severe imbalance of IL-18/IL-18BP in patients with secondary hemophagocytic syndrome. Blood. 2005;106(10):3483-9.

20. Martinon F, Burns K, Tschopp J. The inflammasome: a molecular platform triggering activation of inflammatory caspases and processing of proIL-beta. Molecular cell. 2002;10(2):417-26.

21. Srinivasula SM, Poyet JL, Razmara M, Datta P, Zhang Z, Alnemri ES. The PYRIN-CARD protein ASC is an activating adaptor for caspase-1. The Journal of biological chemistry. 2002;277(24):21119-22.

22. Bauernfeind FG, Horvath G, Stutz A, Alnemri ES, MacDonald K, Speert D, et al. Cutting edge: NF-kappaB activating pattern recognition and cytokine receptors license NLRP3 inflammasome activation by regulating NLRP3 expression. J Immunol. 2009;183(2):787-91.

23. Shoham NG, Centola M, Mansfield E, Hull KM, Wood G, Wise CA, et al. Pyrin binds the PSTPIP1/CD2BP1 protein, defining familial Mediterranean fever and PAPA syndrome as disorders in the same pathway. Proceedings of the National Academy of Sciences of the United States of America. 2003;100(23):13501-6.

24. Yaffe MB, Rittinger K, Volinia S, Caron PR, Aitken A, Leffers H, et al. The structural basis for 14-3-3:phosphopeptide binding specificity. Cell. 1997;91(7):961-71.

25. Yu JW, Wu J, Zhang Z, Datta P, Ibrahimi I, Taniguchi S, et al. Cryopyrin and pyrin activate caspase-1, but not NF-kappaB, via ASC oligomerization. Cell death and differentiation. 2006;13(2):236-49.

26. Van Gorp H, Saavedra PH, de Vasconcelos NM, Van Opdenbosch N, Vande Walle L, Matusiak M, et al. Familial Mediterranean fever mutations lift the obligatory requirement for microtubules in Pyrin inflammasome activation. Proceedings of the National Academy of Sciences of the United States of America. 2016;113(50):14384-9.

27. Ben-Zvi I, Kukuy O, Giat E, Pras E, Feld O, Kivity S, et al. Anakinra for colchicine resistant familial Mediterranean fever - A randomized, double blind, placebo-controlled trial. Arthritis Rheumatol. 2016.

28. Laskari K, Boura P, Dalekos GN, Garyfallos A, Karokis D, Pikazis D, et al. Longterm Beneficial Effect of Canakinumab in Colchicine-resistant Familial Mediterranean Fever. J Rheumatol. 2017;44(1):102-9.

29. Pecher AC, Igney-Oertel A, Kanz L, Henes J. Treatment of familial Mediterranean fever with anakinra in patients unresponsive to colchicine. Scand J Rheumatol. 2017:1-3.

30. Canna SW, Girard C, Malle L, de Jesus A, Romberg N, Kelsen J, et al. Life-threatening NLRC4-associated hyperinflammation successfully treated with IL-18 inhibition. The Journal of allergy and clinical immunology. 2016.

Figures

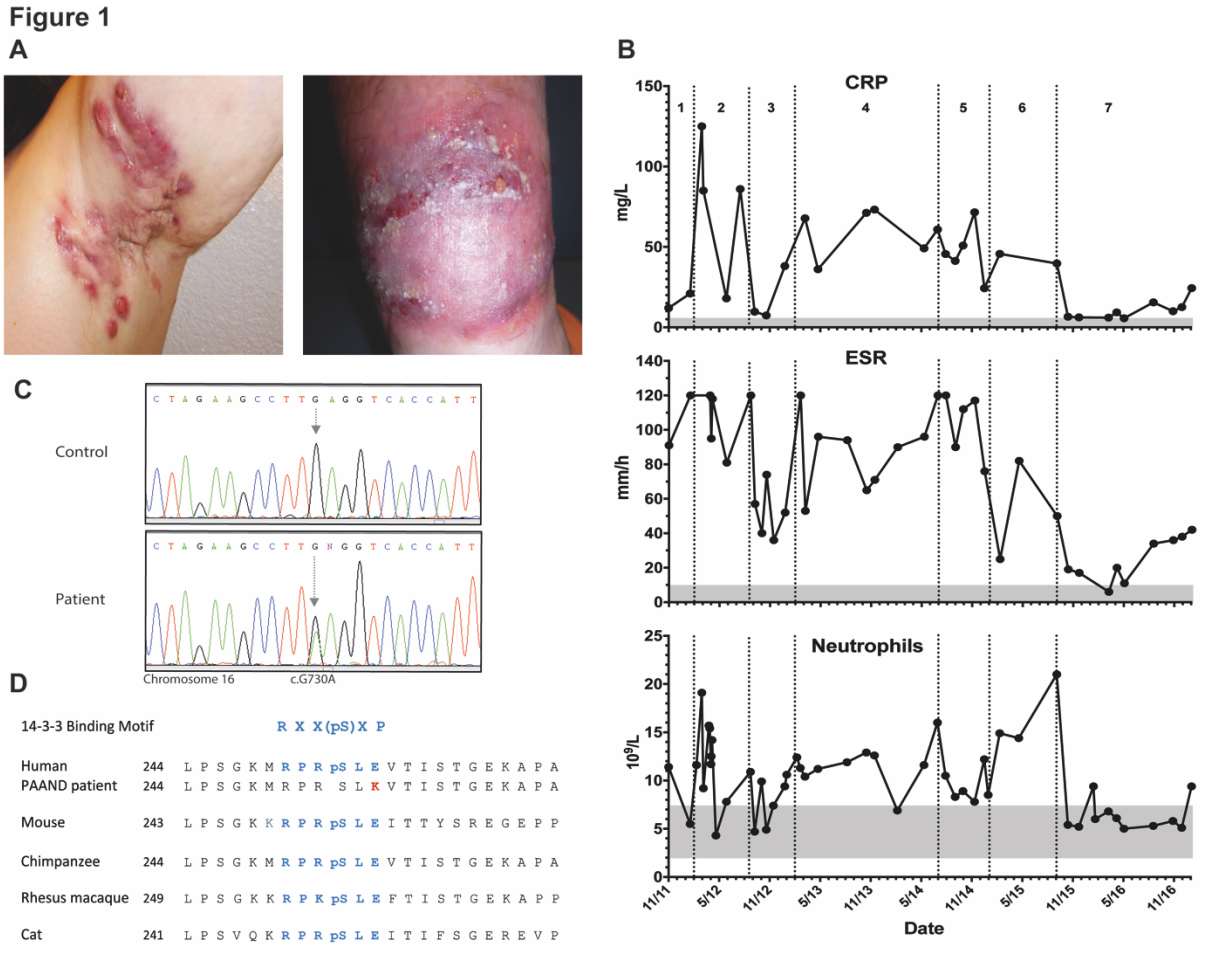

Figure 1. Clinical features of PAAND. (A) Representative macroscopic images of dermatological manifestations in index case (left: hidradenitis suppurativa axillae; right: pyoderma gangrenosum lower leg). (B) Acute phase reactants and neutrophils over time, with treatment periods 1. infliximab + methotrexate; 2. prednisolone + cyclosporin A; 3. prednisolone + infliximab; 4. prednisolone + doxycycline; 5. prednisolone + anakinra + clindamycin; 6. prednisolone + clindamycin + moxifloxacin + dapsone; 7. prednisolone + clindamycin + moxifloxacin + dapsone + adalimumab. (top: C-reactive protein (CRP); middle: Erythrocyte sedimentation rate (ESR); bottom: peripheral blood neutrophil count). (C) DNA chromatogram showing the heterozygous G-to-A transition at position corresponding to c.730 *MEFV*. (D) p.E244 pyrin is highly conserved across species. The glutamate is in position +2 of a 14-3-3 binding motif.

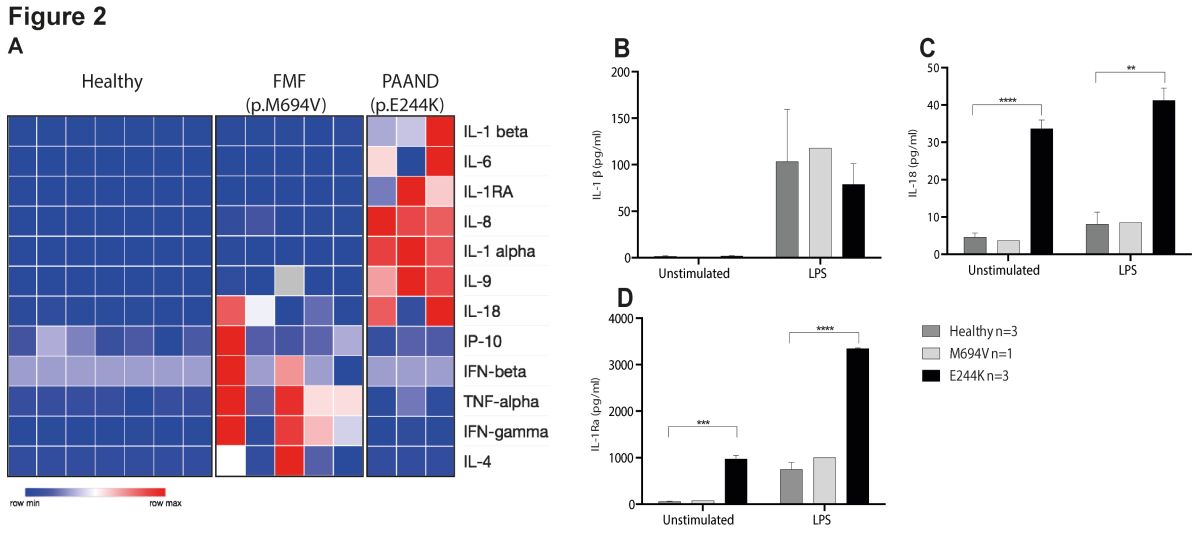

499

500 **Figure 2: PAAND (p.E244K pyrin) has a distinct cytokine and inflammasome profile**
501 **compared with FMF.** (A) Heat map of serum cytokine analysis of healthy controls, patients
502 with FMF and genetically confirmed homozygous p.M694V *MEFV* mutation or patients with
503 PAAND carrying the heterozygous p.E244K *MEFV* mutation. Representative of relative
504 values of minimum and maximum concentrations measured per cytokine. (B) Serum total IL-
505 18 analysis compared with IL-18BP. Assessment of (C) ASC speck forming monocytes by
506 flow cytometry and (D) active caspase-1 by YVAD-FLICA staining. PBMC IL-1β (E), IL-18
507 (F), and IL-1Ra (G) cytokine production at baseline and with LPS stimulation in healthy
508 controls, FMF and PAAND patients. **P <0.05 , **P<0.01, ***P <0.001, ****P <0.0001.*

509

Figure 3

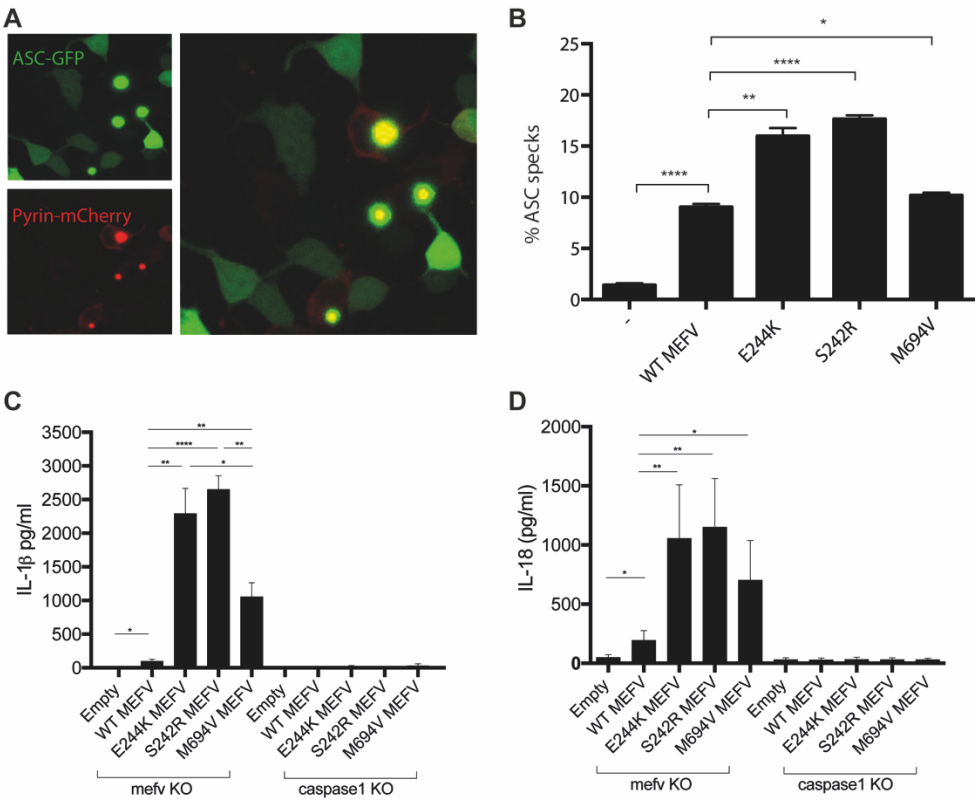

510

511 **Figure 3: Increased inflammasome activation by p.E244K pyrin.** (A) Confocal microscopy
512 showing colocalisation of mCherry-tagged pyrin and GFP-tagged ASC transfected into
513 HEK293T cells. (B) Increase in spontaneous ASC speck formation in p.E244K pyrin compared
514 to WT pyrin or ASC alone control. (C) FACS analysis of HEK293T cells with mCherry-tagged
515 pyrin and GFP-tagged ASC constructs. After 16h, cells were selected by forward scatter (FSC)
516 and side scatter (SSC), expression of both constructs (mCherry and GFP) and finally GFP area
517 versus width. (D) Flow cytometric quantification of ASC speck formation for WT and various
518 pyrin mutants. Data pooled from three independent experiments. *$P < 0.05$, **$P < 0.01$, ****P
519 < 0.0001.

520

Figure 4

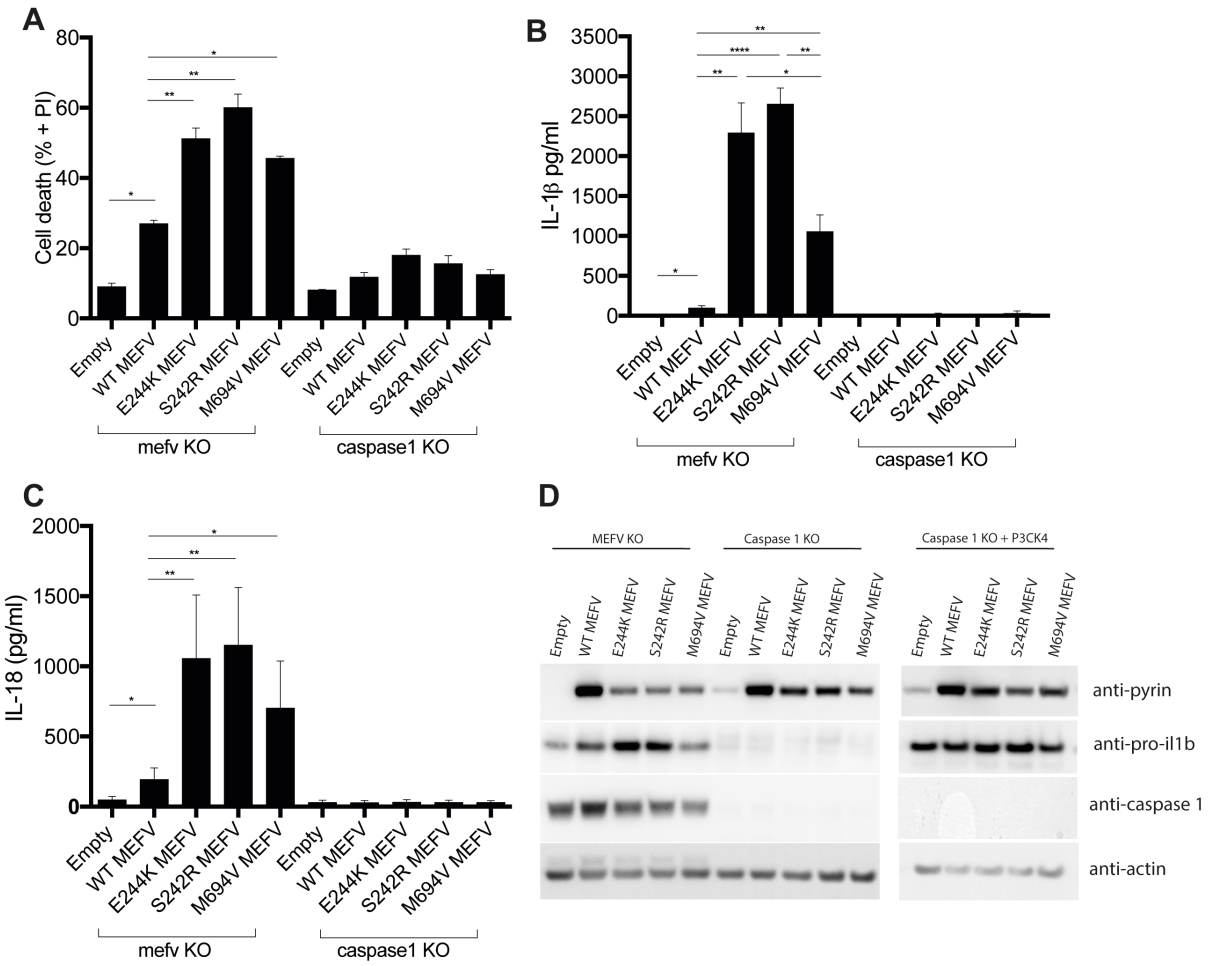

Figure 4: Pyroptosis and cytokine production by p.E244K pyrin. Monocytic THP1 cells with pyrin or caspase-1 deleted by CRISPR were reconstituted with WT and mutant pyrin using lentiviral vectors. (A) Cell death was measured by propidium iodide (PI) staining and flow cytometry, and (B) IL-1β and (C) IL-18 measured by ELISA 48h after lentiviral infection. The increased cell death (A), IL-1β (B) and IL-18 (C) seen in the pyrin mutants was abrogated in the caspase-1 KO THP1 cells. (D) Whole cell lysate was prepared from THP-1 cells and western blotting was performed, probing for pro-IL-1β to determine the mechanism of the IL-1β response. *CASP1* KO cells were further treated with Pam3CSK4 to look at a physiologic priming response to ensure that pro-IL-1β could be generated in this cell line. Data pooled from three independent experiments. *$P < 0.05$, **$P < 0.01$, ***$P < 0.001$, ****$P < 0.0001$.

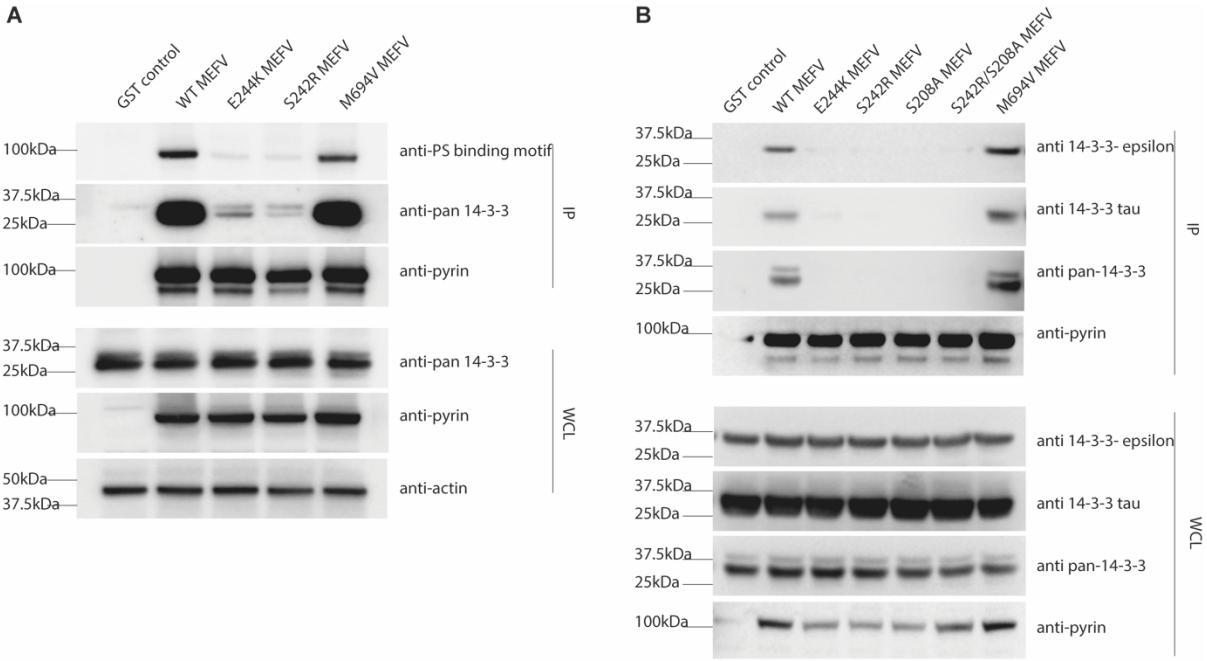

532

533 **Figure 5: Reduced 14-3-3 binding by p.E244K pyrin.** HEK293T cells were transfected with
534 GST-tagged pyrin, with or without PAAND and FMF mutations, and immunoprecipitation
535 performed. (A) Western blot was performed to compare phosphoserine 14-3-3 binding motif,
536 pan-14-3-3 binding and pyrin expression in immunoprecipitate (IP) and whole cell lysate
537 (WCL). Comparison was made to p.S242R and p.M694V pyrin. (B) Western blot was
538 performed to compare pan-, τ or ε 14-3-3 binding and pyrin expression in IP and WCL.
539 Comparison was made to p.S242R, p.S208A, p.S208A/S242R and p.M694V pyrin.
540 Representative of three independent experiments.

541

Figure 6

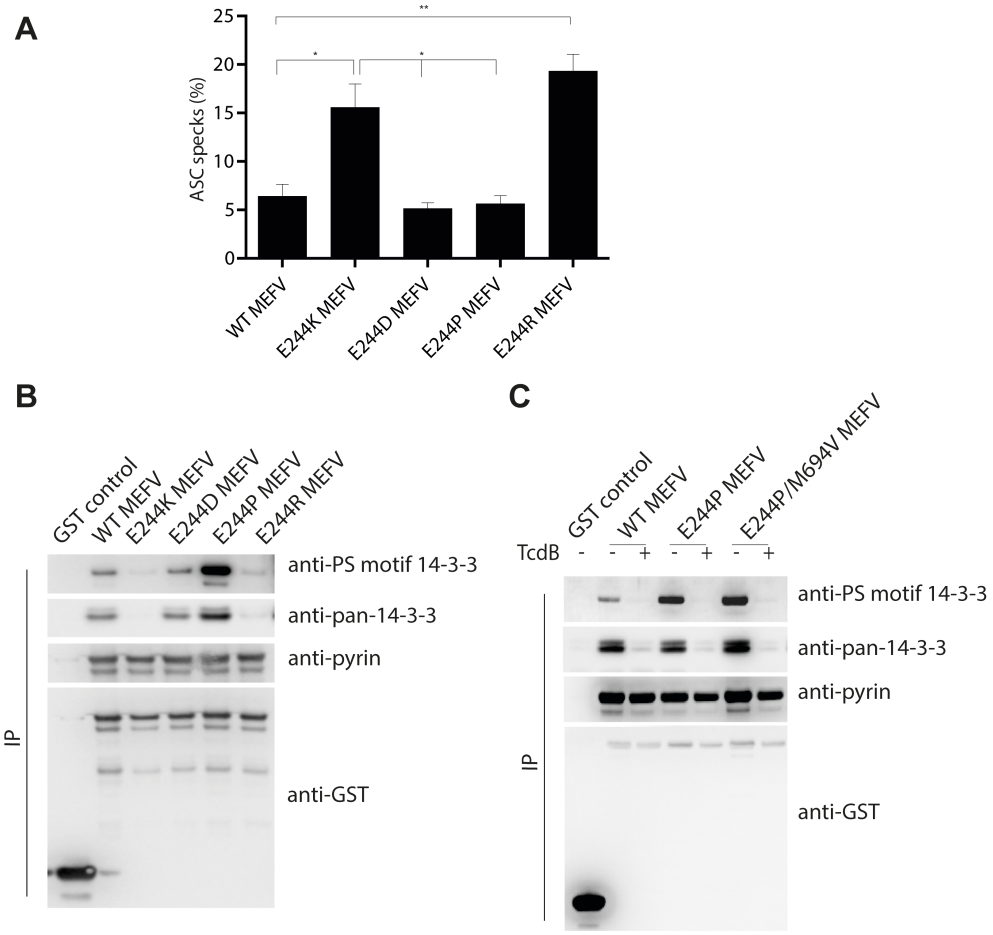

542

543 **Figure 6: +2 position of 14-3-3 binding site is important in regulation of pyrin activation**.
544 (A) Flow cytometric analysis of ASC speck formation performed on HEK293T cells
545 transfected with mCherry-tagged pyrin with various mutations at position p.E244 and GFP-
546 tagged ASC. Data pooled from three independent experiments. (B) HEK293T cells were
547 transfected with GST-tagged pyrin with various mutations at position p.E244, and then
548 immunoprecipiated and blotted with antibodies to detect the phosphorylated 14-3-3 binding
549 motif, pan-14-3-3, pyrin or the GST tag. (C) Immunoprecipitation was performed as described
550 above, but with TcdB stimulation for 16h, to assess phosphorylation of 14-3-3 binding sites
551 and 14-3-3 binding. Representative of three independent experiments. *$P < 0.05$, **$P < 0.01$

Supplementary Figures

Supplementary Figure 1

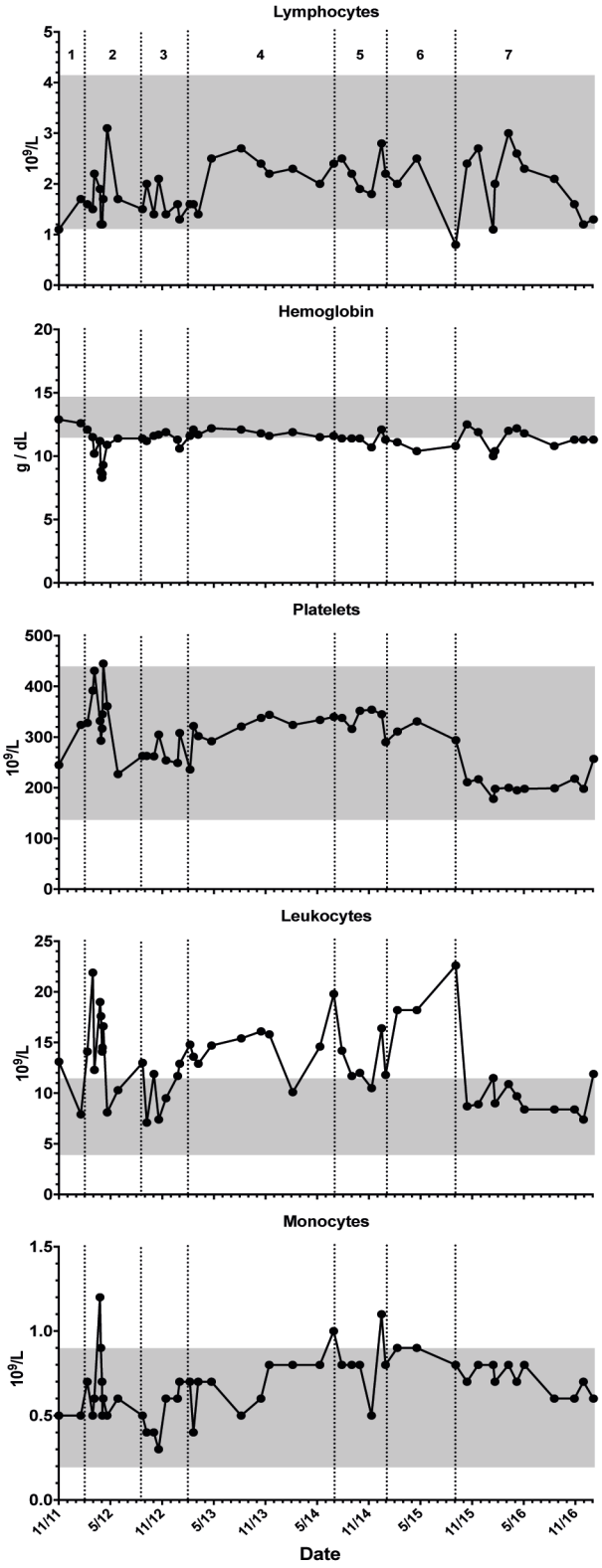

Supplementary Figure 1: Further clinical information. Haematological and biochemical data of index case charted across time, with treatment periods 1. infliximab + methotrexate; 2.

prednisolone + cyclosporin A; 3. prednisolone + infliximab; 4. prednisolone + doxycycline; 5. prednisolone + anakinra + clindamycin; 6. prednisolone + clindamycin + moxifloxacin + dapsone; 7. prednisolone + clindamycin + moxifloxacin + dapsone + adalimumab.

Supplementary Figure 2

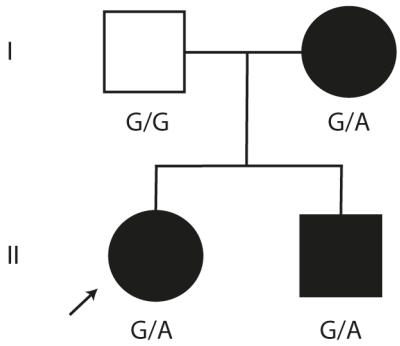

Supplementary Figure 2: Pedigree of the family. Solid symbols (squares=male, circles=females) denote affected individuals. Open symbols denote unaffected individuals. The arrow indicates the proband of the family.

Control number	Genotype	Symptomatic	Treatment	CRP (<10mg/L)
1	M694V/M694V	No	Colchicine	12.7
2	M694V/M694V	No	Colchicine	20.3
3	M694V/M694V	No	Unknown	3.2
4	M694V/M694V	No	Unknown	70.9
5	M694V/M694V	No	Unknown	45.2

Supplementary Table 1: Summary of FMF controls. Table of FMF controls on whom serum cytokines assessed. All patients were asymptomatic but four of five had evidence of subclinical inflammation.

571

Supplementary Figure 3

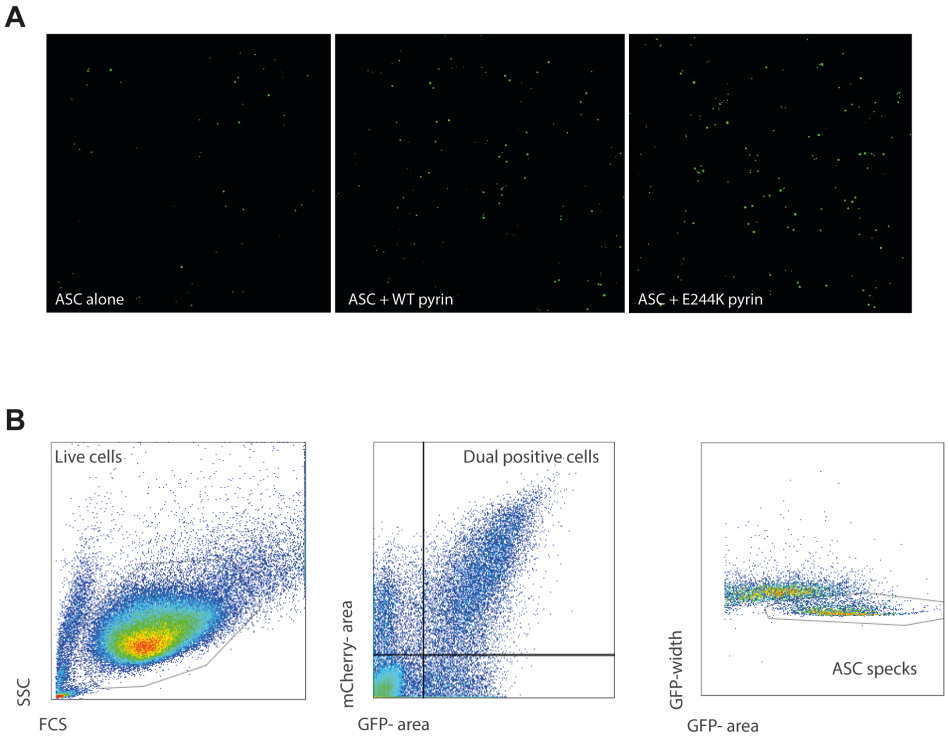

572

573 **Supplementary Figure 3: ASC Speck analysis.** (A) Larger field of view of

574 immunofluorescence showing background ASC speck formation, and an increase with WT

575 and pyrin p.E244K transfection. (B) Gating strategy for quantification of ASC speck

576 formation. HEK293T cells were gated on forward and side scatter, selecting live cells. Dual

577 GFP and mCherry positive cells were selected. ASC specks were determined by reduced

578 width and increased area of GFP signal.

Supplementary Figure 4

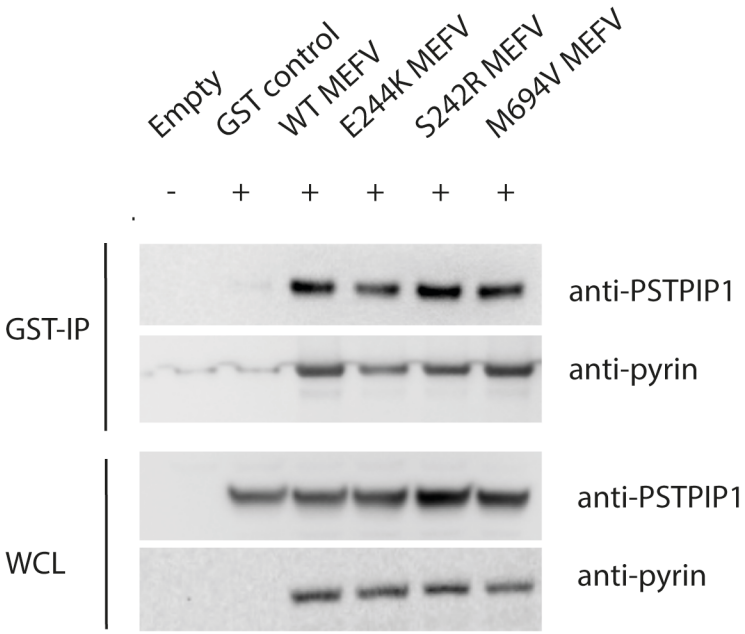

579

580 **Supplementary Figure 4: Binding of PSTPIP1 to PAAND pyrin is unaltered.** HEK293T
581 cells were transfected with GST-tagged pyrin, with or without PAAND and FMF mutations,
582 in addition to WT PSTPIP1. GST-immunoprecipitation performed and comparison of PSTPIP1
583 binding to various MEFV constructs made. Representative of three independent experiments.

584

585